Modern Physics Letters B
Vol. 28, No. 6 (2014) 1450044 (13 pages)
© World Scientific Publishing Company
DOI: 10.1142/S0217984914500444

World Scientific
www.worldscientific.com

Optimizations of inductively coupled plasma etching and design for sensing window of Mach–Zehnder interferometer sensor in polymer technology

Tianfu Yang, Tianjiao Wang, Chuantao Zheng, Xibin Wang and Daming Zhang*

State Key Laboratory on Integrated Optoelectronics,
College of Electronic Science and Engineering, Jilin University,
2699 Qianjin Street, Changchun 130012, China
**zhangdm@jlu.edu.cn*

Received 8 December 2013
Revised 12 January 2014
Accepted 20 January 2014
Published 25 February 2014

The inductively coupled plasma etching parameters for fabricating sensing windows of integrated Mach–Zehnder interferometer sensor based on polymers are systematically investigated. Under the optimum etching condition, we fabricate an improved sensing waveguide with three sensing surfaces, whose sensitivity can be enhanced by a factor of 3.5 in theory. Through precisely controlling the etching time, low propagation loss and high hydrophilicity are both achieved in the etched sensing waveguide. This optimizing approach along with rapid response and stable operation has rendered the MZI waveguide sensor more competent to practical requirements of RI sensing and biochemical sensing.

Keywords: Integrated optical waveguide sensor; Mach–Zehnder interferometer; inductively coupled plasma etching; sensitivity enhancement.

1. Introduction

For the past few years, thinned fibers have been intensively used in refractive index (RI) sensing applications.[1,2] However, the ultimate goal for the development of biochemical sensors in food safety, health care, environmental protection and national defense is the implementation of lab-on-chip (LOC) for micro total analysis systems (μ-TAS).[3] The integrated optical waveguide sensors (IOWS) are preponderant in miniaturization, multiple detection and function, structure design and material selection. Accordingly, various IOWS in different structures have been reported until

*Corresponding author.

Mod. Phys. Lett. B 2014.28. Downloaded from www.worldscientific.com
by UNIVERSITY OF TORONTO on 03/31/14. For personal use only.

www.sbm.com.cn

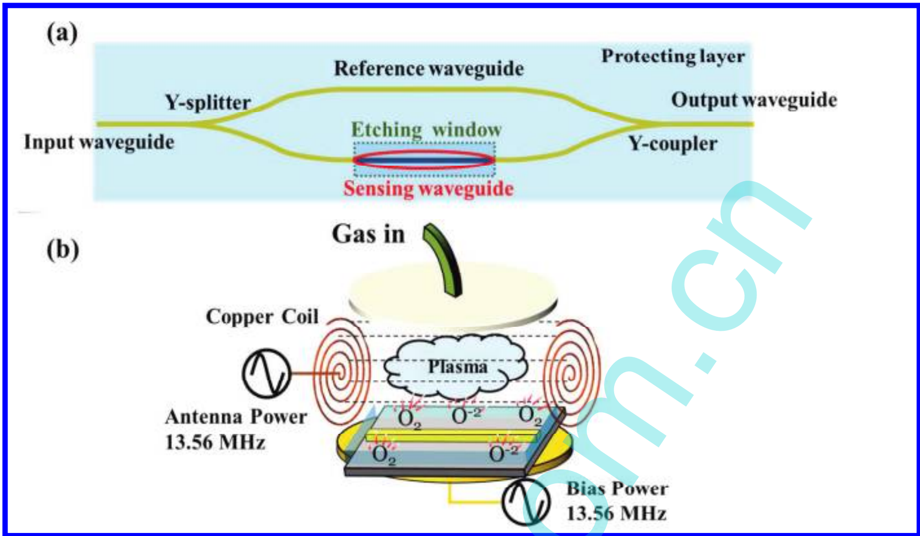

Fig. 1. The schematic of (a) a MZI waveguide sensor with sensing window; (b) ICP etching for the fabrication of sensing window.

Mod. Phys. Lett. B 2014.28. Downloaded from www.worldscientific.com by UNIVERSITY OF TORONTO on 03/31/14. For personal use only.

www.spm.com.cn

recently, such as surface plasmon resonator,[4] microring resonator,[5] long period grating[6] and Mach–Zehnder interferometer (MZI).[7–10] Among these sensors, the MZI sensor has always been one of the biggest concerns in several decades by virtue of an internal reference minimizing the perturbations of environmental fluctuation, as well as a large sensing area.

In MZI sensing configurations [as shown in Fig. 1(a)], an open sensing window fabricated by dry etching technology, e.g. inductively coupled plasma (ICP) etching [as depicted in Fig. 1(b)], is of great importance for sensing applications. As for MZI sensor based on inorganic materials, while fabricating sensing windows, sulfur hexafluoride (SF_6) and carbon tetrafluoride (CF_4) are specifically utilized as etching gases, but both of them are highly toxic and much more expensive than O_2 or other common etching gases. Moreover, it is inappropriate for inorganic sensing arms to be immobilized by chemical bonds on their surfaces, which is necessary in LOC applications. Therefore, the fabrication of sensing window in polymer technology promises an opportunity to realize cost-effective mass production and better sensing performance for MZI sensor. Accordingly, our research select cost-effective polymers as waveguide core/cladding materials and comprehensively investigate on the ICP etching parameters for fabricating sensing window in MZI refractive sensor, which aims to shape a low-loss, three-dimensional (3D) sensing arm with highly hydrophilic surfaces contributing to a closer interaction between guiding light and test solutions. Characterizations by atomic force microscopy (AFM), scanning electron microscopy (SEM) and measurements of water contact angle and transmission loss have confirmed our presumption. At last, a polydimethylsiloxane (PDMS) microfluidics channel is attached to the sensor chip to access flow stabilities of analytes and

monitor the kinetics of transient processes in real time.[11] With the help of the above optimizations, the polymeric MZI waveguide sensor could be more competent to practical sensing applications.

2. Design and Optimization

The phase θ of the guiding mode in sensing waveguide depends linearly on its effective RI N_{eff}. And it can be expressed as

$$\theta = \frac{2\pi}{\lambda} \times L \times N_{\text{eff}}\,, \tag{1}$$

where λ is the operation wavelength, and L is the waveguide length. The sensitivity of a waveguide sensor can be defined as the ratio of the effective RI change of the guiding mode to the RI variation of the core layer surroundings, n_c:

$$S = \frac{\partial\theta}{\partial n_c} = \left(\frac{2\pi L}{\lambda}\right)\left(\frac{\partial N_{\text{eff}}}{\partial n_c}\right). \tag{2}$$

For the schematic cross-section of a conventional sensing window in waveguide sensors shown in Fig. 2(a), only the upper surface is exposed to the measurands. The reasons for this case generally lie in the unsuited match of core and cladding materials for etching process or the inverted-rib waveguide structure.[7,9] Obviously,

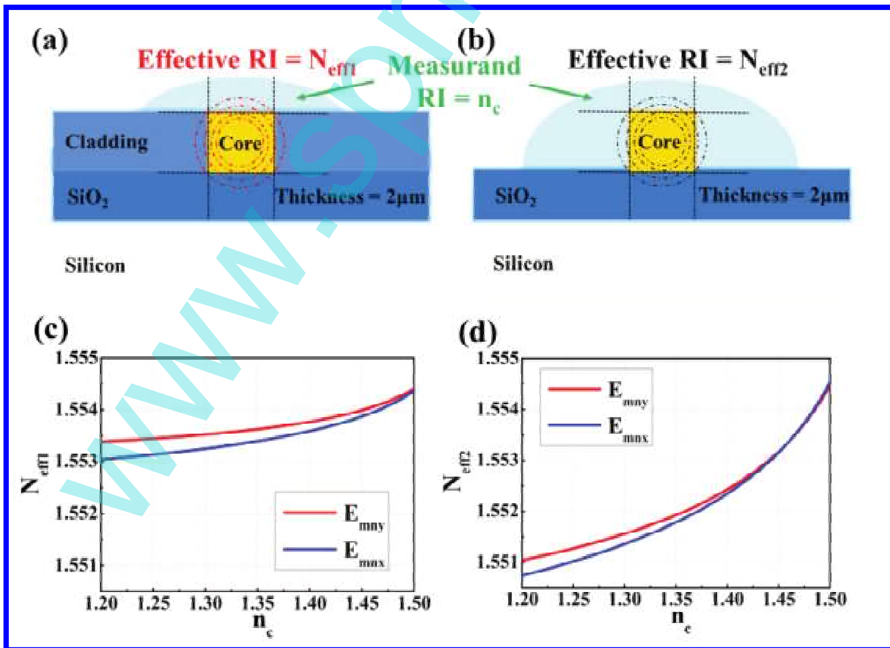

Fig. 2. (Color online) The schematic of (a) a conventional structure of sensing window; (b) an improved 3D structure of sensing window; (c), (d) calculated effective RI N_{eff1} and N_{eff2} for TM_0 and TE_0 modes in conventional and improved sensing windows, respectively, as a function of the RI of analyte, n_c.

Mod. Phys. Lett. B 2014.28. Downloaded from www.worldscientific.com
by UNIVERSITY OF TORONTO on 03/31/14. For personal use only.

www.spm.com.cn

it is insufficient for the evanescent field to penetrate into surrounding measurands. In order to improve the sensing performance, we propose an advantageous sensing window exposing more area in per unit length, as shown in Fig. 2(b). Such model could be accomplished through dry etching process. Through the optimal etching parameters, we readily remove the entire protective layer in the sensing area so that three sides of the rectangular sensing arm are accessible to analytes, forming a 3D structure. Without any cladding covering on it, this 3D structure assures a stronger evanescent field in the sensing arm.

To analyze the change of effective RI N_{eff1} for conventional structure and N_{eff2} for 3D structure corresponding to n_c, we calculated the functions in the two structures, respectively. The parameters used for calculation are given as follows: range of measurands index, 1.200 to 1.500; SiO_2 under cladding index, 1.462; core layer size and RI, 3 μm $\times$ 3 μm and 1.571; poly(methyl methacrylate–glycidyl methacrylate) [P(MMA-GMA)] cladding index, 1.495. Calculation results are shown in Figs. 2(c) and 2(d). The N_{eff2} increases much more dramatically than N_{eff1} both at TE_0 and TM_0 modes. The ratio of $\Delta N_{\mathrm{eff2}}/\Delta n_c$ to $\Delta N_{\mathrm{eff1}}/\Delta n_c$ is 3.5, equaling that the sensitivity of a conventional structure of waveguide sensor could be increased by 3.5 times, just with this significantly enlarged sensing area.

3. Experimental Method

3.1. *Device fabrication*

The waveguide of our MZI sensor was formed by silica, SU-8 and P(MMA-GMA) three-layer structure. The polymer SU-8 2005 (microChem, MA, USA), was used as the core material. A low-cost copolymer P(MMA-GMA) synthesized in our lab was applied as the protecting layer covering the sensor chip except the sensing window. A 2.0 μm-thick silica layer was grown on the silicon substrate as the under cladding. The detailed fabrication process of the sensor chip is shown in Fig. 3:

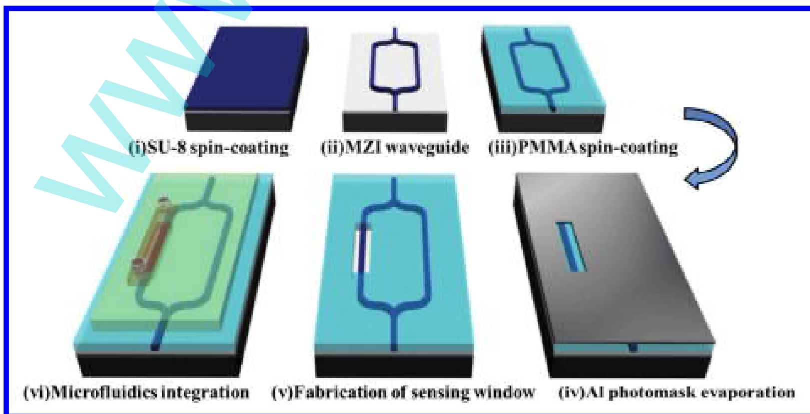

Fig. 3. Fabrication process of the MZI waveguide sensor chip.

Mod. Phys. Lett. B 2014.28. Downloaded from www.worldscientific.com by UNIVERSITY OF TORONTO on 03/31/14. For personal use only.

www.spm.com.cn

(i) SU-8 2005 was spin-coated on a silicon substrate with a 2 μm silicon dioxide layer at a spinning rate of 4000 r/min and soft baked at 65°C for 15 min, 90°C for 20 min to form a 3 μm film as the light-guiding layer;
(ii) the coated wafer was exposed to an UV light emitting at a wavelength of 360 nm for 8 s and post baked at 65°C for 15 min and 95°C for 15 min. After that, it was developed for 35 s in SU-8 developer. At this point, the waveguide core with a square cross-section was formed;
(iii) P(MMA-GMA) was spin-coated on the SU-8 core as the upper cladding and thermally cured at 120°C for 2.5 h;
(iv) a 100 nm-thick film of aluminum was evaporated on top of the upper cladding and patterned by photolithography;
(v) we fabricated the designed sensing window by ICP etching under the optimum parameters, in consideration of the two etching rates and surface roughnesses of core and cladding materials. After the above steps, the MZI waveguide with a sensing window was successfully fabricated;
(vi) a PDMS flow chamber was mounted on it, which allows rinsing different solutions over the sensing arm of the MZI.

3.2. *Sample characterization*

Characterizations of AFM and SEM were utilized to optimize etching parameters. AFM images were recorded with a multimode scanning probe microscope CSPM5000 (Being Nano-Instrument Ltd., China) that operated in contact mode with an AFM probe in the model of Contact-G (Innovative Solutions Bulgaria Ltd., Bulgaria). The morphological characterization of the etched window was examined by means of SEM JSM-7600F (JEOL Ltd., Japan) that operated on a voltage of 5 kV. For investigating the influence on the hydrophily of sensing waveguide after etching, water contact angle was measured using a Contact Angle System OCA20 instrument (DataPhysics Instruments GmbH, Germany) at ambient temperature. A high purity water droplet ($\sim$5 μL) was deposited on the sample surface and the static equilibrium water contact angle was measured immediately upon needle removal. All tests were repeated at least three times on one sample for reducing errors, as well as in AFM measurements.

4. Results and Discussion

Our etching for sensing window was carried out in an ICP etching system CE-300I (ULVAC Co. Inc., Japan) using oxygen and argon plasmas. Radio frequency (RF) power of 13.56 MHz was supplied to the single-turn antenna through a matching box and coupled via a quartz window at top of the chamber. The RF power generated at the antenna affected the plasma density, while keeping electrons temperature constant. The sample was placed on a He-cooling stage and biased by RF (13.56 MHz) power which provided the ion energies. The distance between the excited plasmas and sample is only a few of mean free paths, so high-density plasmas without energy loss are accessible. In our research, two main steps constituted

Mod. Phys. Lett. B 2014.28. Downloaded from www.worldscientific.com
by UNIVERSITY OF TORONTO on 03/31/14. For personal use only.

www.spm.com.cn

the etching process. First, the P(MMA-GMA) cladding covering sensing arm was completely removed. On account of biochemical sensing tests, analytes are generally diluted in buffer solutions, then transported to contact with sensitive elements and it is impossible to obtain a satisfying result with a hydrophobic sensor in experiments. Second, the bare SU-8 waveguide would be under the ICP treatment with additional several tens of seconds in order to form reactive oxygen group such as hydroxyl and carboxyl on its surfaces. Both of the two steps must be carefully controlled in timekeeping under the optimal etching parameters. Since the etched waveguide surface and vertical profiles are both affected by physical bombardment which helps to break chemical bonds, cause lattice damages, increase the adhesion of plasmas, accelerate the stripping of products and promote chemical reactions on the surface of sample.[12] Therefore, we proposed a systematic investigation to acquire a group of optimal etching parameters, including chamber temperature and pressure, antenna power, bias power, gas flow rate and etching time for fabricating the designed sensing window.

Mod. Phys. Lett. B 2014.28. Downloaded from www.worldscientific.com
by UNIVERSITY OF TORONTO on 03/31/14. For personal use only.

4.1. *The effect of chamber temperature and pressure*

The effects of chamber temperature on the etching rate and surface roughness of P(MMA-GMA), which was used as upper cladding in our MZI sensors, were first investigated. Under the pressure of 0.5 Pa, oxygen gas flow of 30 sccm and etching time of 150 s, the experiments were operated with three combinations of antenna power and bias power [as shown in Figs. 4(a) and 4(b)]. From Figs. 4(a) and 4(b), as the temperature went up from 10°C to 40°C on one side, none of the three roughnesses obviously decreased. It had no positive effect on raising chamber

www.spm.com.cn

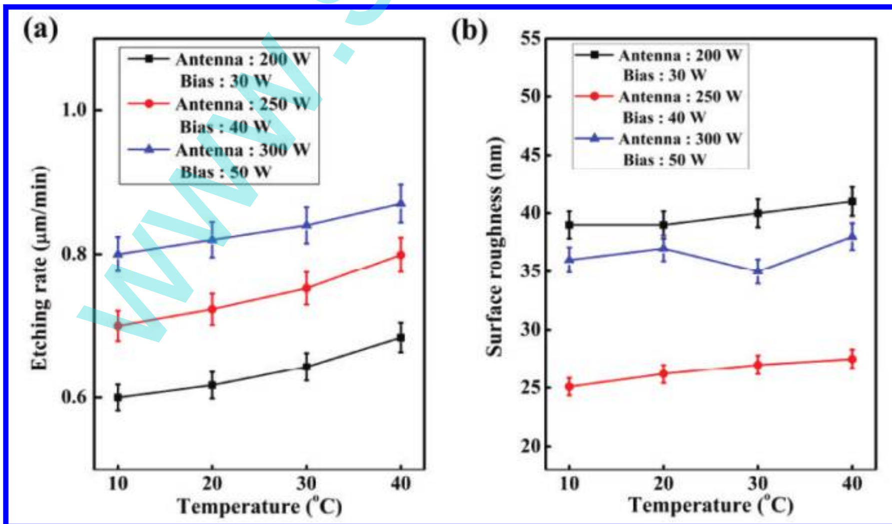

Fig. 4. The effects of temperature on (a) etching rate; (b) surface roughness for P(MMA-GMA) etching.

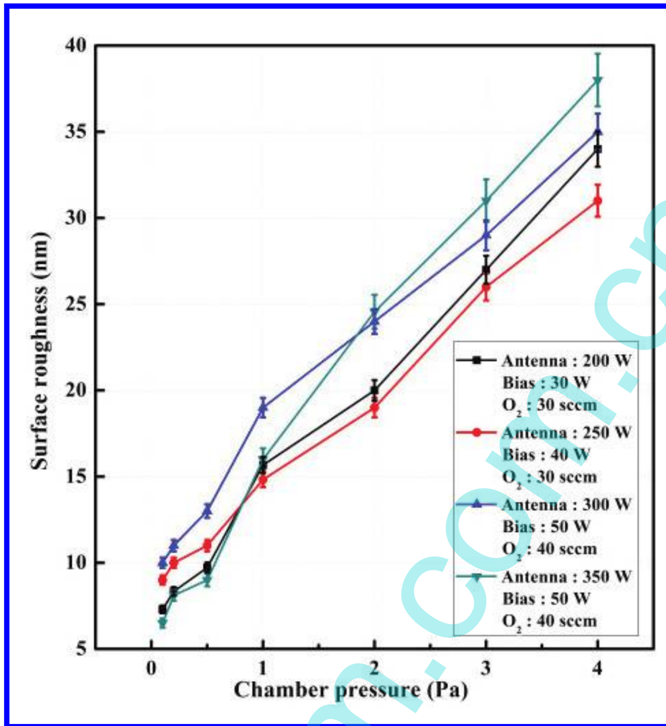

Fig. 5. Surface roughness of P(MMA-GMA) upper cladding as a function of chamber pressure.

Mod. Phys. Lett. B 2014.28. Downloaded from www.worldscientific.com
by UNIVERSITY OF TORONTO on 03/31/14. For personal use only.

www.som.com.cn

temperature to improve surface morphology. On the other side, low temperature affected molecular movements of plasmas, which lead to the reductions of all the three etching rates. For a moderate etching rate, we consider that the temperature in the range of 20°C to 30°C is suitable to our etching application.

Second, four random combinations of three etching parameters (as shown in Fig. 5) under the pressure ranging from 0.1 Pa to 4 Pa were applied to explore a universally applicable relationship between chamber pressure and surface roughness in the P(MMA-GMA) etching process. At the pressure below 1 Pa, none of the four conditions resulted in unacceptable surface roughness. However, the surface under the four conditions increased sharply without exception when the pressure was higher than 1 Pa. During the etching process, while etching gases flowing into the chamber, external electric field drove the free electrons in the etching gases to proceed advance and return movements impacting atoms and molecules. Through the impacting, more free electrons were released to replenish energies for the ions. Those atoms and molecules, free electrons and ions gathering in the central of the chamber constituted plasmas. Regardless of the other three parameters, such impacting was weakened owing to the energy loss of free electrons when the chamber pressure was higher than 1 Pa, which resulted to low-density plasmas. Therefore, in consideration of the roughness, a chamber pressure of 0.5 Pa was preferable to obtain smoother surfaces.

Mod. Phys. Lett. B 2014.28. Downloaded from www.worldscientific.com
by UNIVERSITY OF TORONTO on 03/31/14. For personal use only.

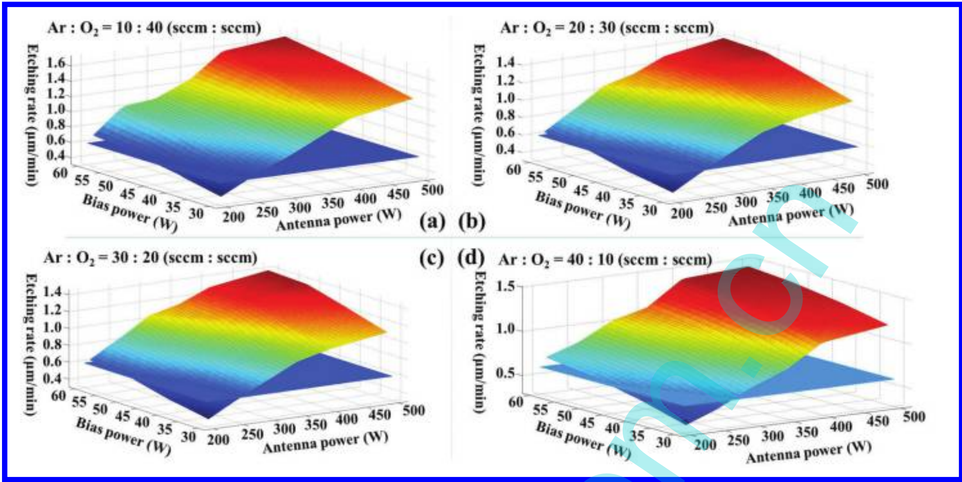

Fig. 6. (Color online) The effects of etching parameters on the P(MMA-GMA) upper cladding.

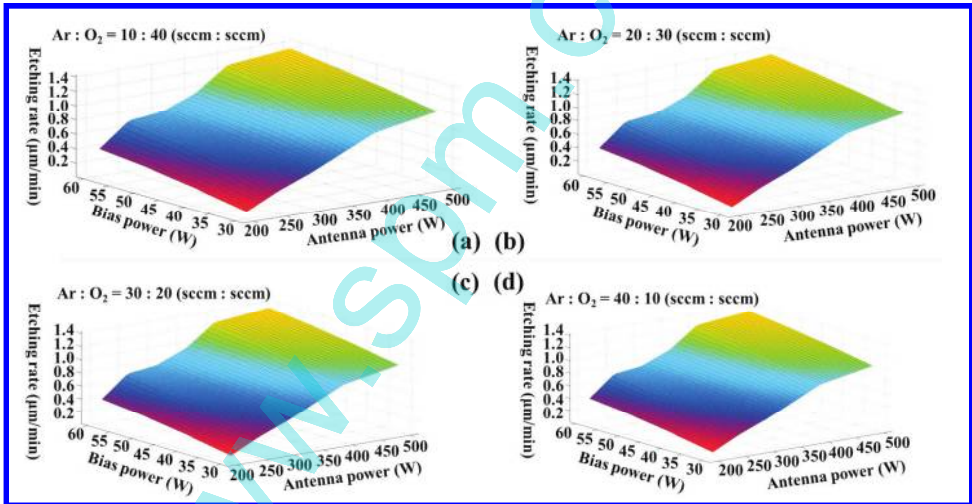

Fig. 7. (Color online) The effects of etching parameters on the SU-8 core.

4.2. *Optimization of etching conditions for step one*

For the purpose of low propagation loss and 3D structure, we considered the two etching rates of P(MMA-GMA) and SU-8 2005 as 0.6 μm/min and minimal, respectively. To realize this situation, the antenna power was varied from 200 W to 500 W, the bias power changed from 30 W to 60 W and the ratio of flow rate of Ar to O_2 set as 10:40, 20:30, 30:20 and 40:10 (sccm:sccm). So the etching parameters of our experiments for the investigation of the two etching rates were the permutation and combination of the three group of variables. All experimental results were collected for statistical processing, as shown in Figs. 6 and 7. Simply, and

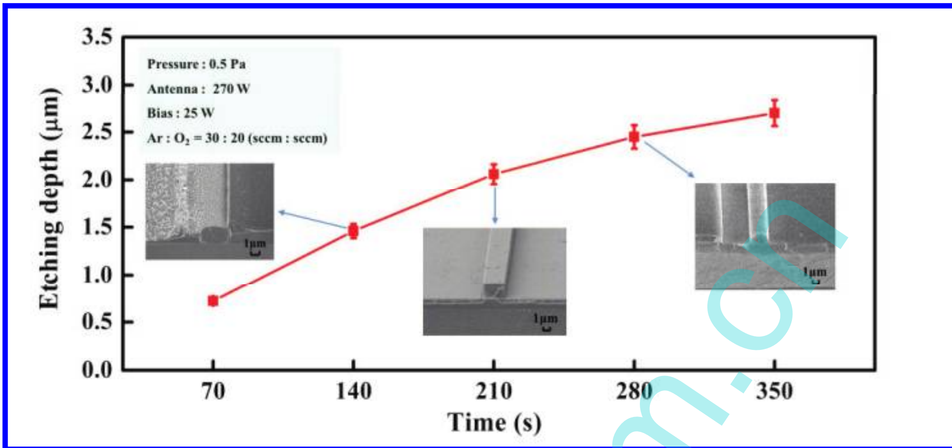

Fig. 8. Etching depth of the sensing window as a function of etching time.

Mod. Phys. Lett. B 2014.28. Downloaded from www.worldscientific.com
by UNIVERSITY OF TORONTO on 03/31/14. For personal use only.

www.spm.com.cn

such method equaled that three variables (antenna power, bias power and gases) were inputted into a system and two output (two etching rates of P(MMA-GMA) and SU-8 2005) resulted. Based on this principle, the optimal etching condition was found by calculation and characterization of AFM and SEM. According to the above evaluations, the etching conditions of a 0.5 Pa chamber pressure, a 270 W antenna power, a 25 W bias power, and a 30:20 (sccm:sccm) ratio of flow rate of Ar to O_2 were considered appropriate for the ICP etching of fabricating sensing window.

To testify the optimal etching parameters, the etching depth of the upper cladding as a function of time was studied in Fig. 8. From the SEM image shown as the left inset in Fig. 8, we found that a 140 s etching could not remove the P(MMA-GMA) completely. After 70 s, the picture of SEM as the middle inset in Fig. 8 indicated that no upper cladding was remained, which meant that the first step of ICP etching for removing the protective layer was accomplished. We continued the etching process so that the waveguide core of SU-8 2005 was transformed due to the over-etching, as shown in the right inset of the SEM image.

4.3. *Improvement on hydrophilicity of sensing arm for step two*

For further precisely controlling the second ICP etching step of the improvement of hydrophily, we measured the water contact angle and surface roughness of the sensing waveguide within the etching time from 195 s to 225 s. During these 30 s, the second step would take place. From Fig. 9, as the etching time went on, we could find that the water contact angle decreased from 130° to 30° meanwhile, the surface roughly increased from 32 nm to 58 nm. The oxygen plasmas in ICP etching brought in the immobilization of oxygenous chemical bonds which were hydrophilic groups resulting in high hydrophily on the surfaces of sensing arm. But the water contact angle stayed largely constant while the surface roughness remarkably increased

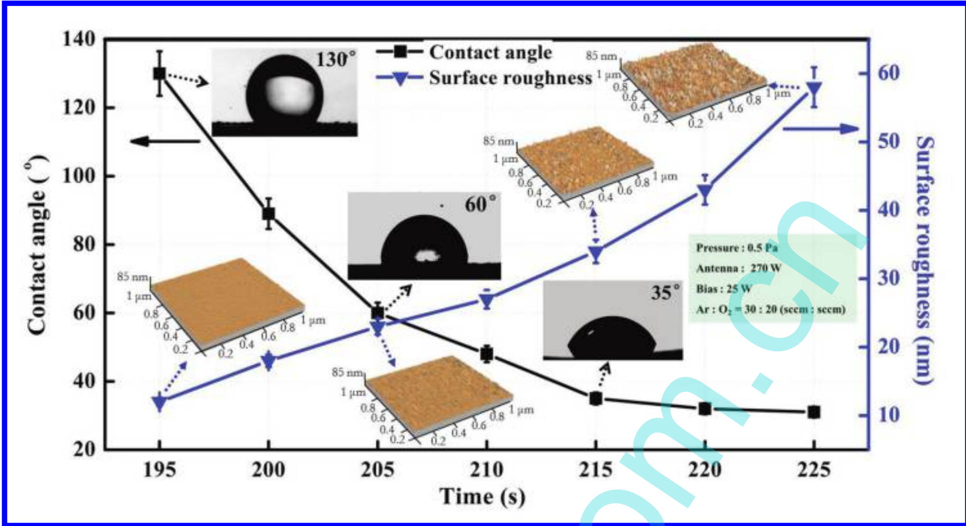

Fig. 9. Water contact angle and surface roughness of the SU-8 2005 sensing waveguide core as a function of etching time.

after a 215 s etching. Judging from the above characterizations such as the insets of images of water contact angle and AFM in Fig. 9, we chose the etching time of 215 s as a suitable parameter for the requirements of the whole etching process.

4.4. *Measurement of transmission loss*

In order to verify that whether our proposed etching process introduced additional loss to damage the transmission of light in the etched waveguide, we measured the propagation loss of sensing waveguide by the cut-back method before and after the etching of sensing window and made a comparison. In the optical test, the light beam (at 1550 nm) produced by a tunable semiconductor laser (TSL-210, Santec) was coupled directly into the input port by a single-mode fiber. At the output of the sensor chip, the transmitted light was coupled into an optical power meter, the readout of which would be collected by the computer connected with it, as shown in the inset of Fig. 10. Figure 10 shows the relation between the insertion loss and waveguide lengths of the two waveguides. No distinct change could be observed between the insertion losses of the two waveguides in several lengths, especially the length ranging from 1 cm to 2.5 cm, which was the typical dimension in applications. The transmission loss before and after etching were estimated as 1.627 dB/cm and 1.678 dB/cm, respectively. We could conclude that the effects on transmission loss or insertion loss induced by the optimized etching process were negligible.

4.5. *Sensing performance*

Different from the optical measurement, a PDMS flow chamber was attached to the sensor chip and connected to a peristaltic pump as well as to the sample fluid

Mod. Phys. Lett. B 2014.28. Downloaded from www.worldscientific.com
by UNIVERSITY OF TORONTO on 03/31/14. For personal use only.

www.spm.com.cn

Mod. Phys. Lett. B 2014.28. Downloaded from www.worldscientific.com
by UNIVERSITY OF TORONTO on 03/31/14. For personal use only.

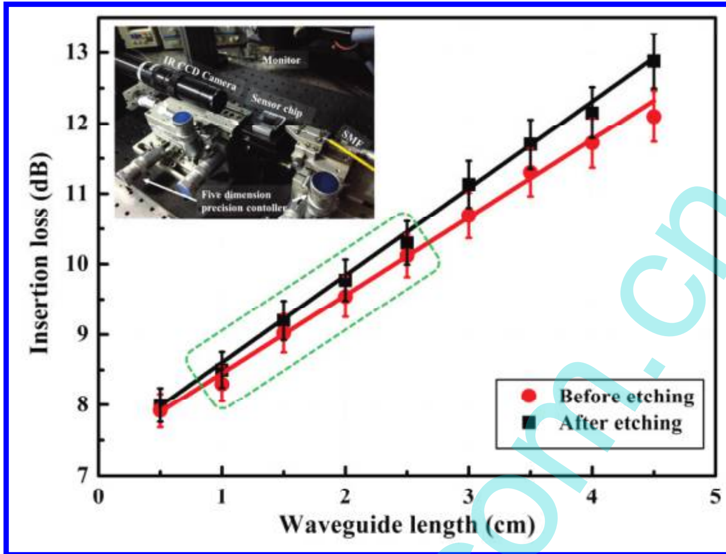

Fig. 10. Comparison of propagation loss of the waveguide before and after etching for fabrication of sensing window.

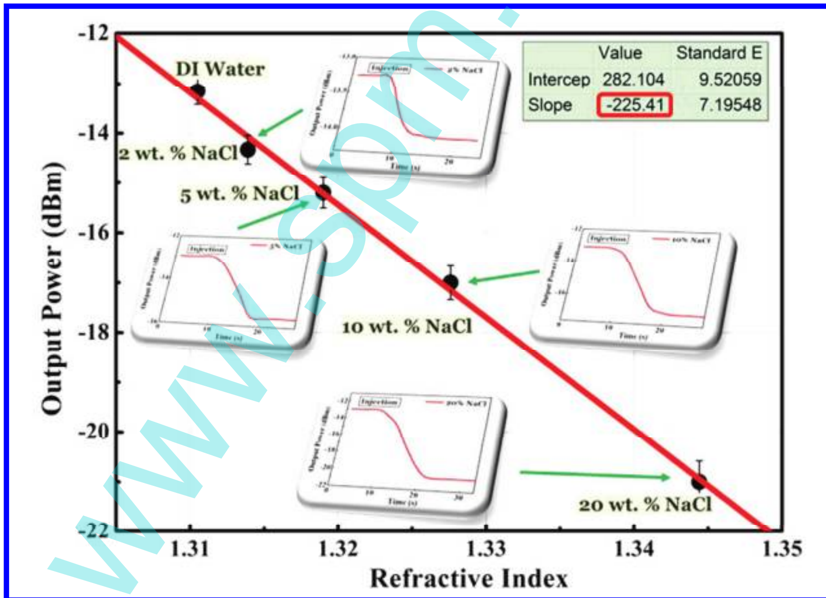

Fig. 11. Calibration of sensitivity of the sensor chip.

reservoirs. First, the DI water was pumped into the flow channels when the signal light through the sensor was stable. The output power of the sensor chip versus the RI are plotted and fitted in Fig. 11. The slope of the fitting line could be regarded as the sensitivity, and we can see that the sensitivity of this MZI waveguide sensor is 225.4 dB/RIU.

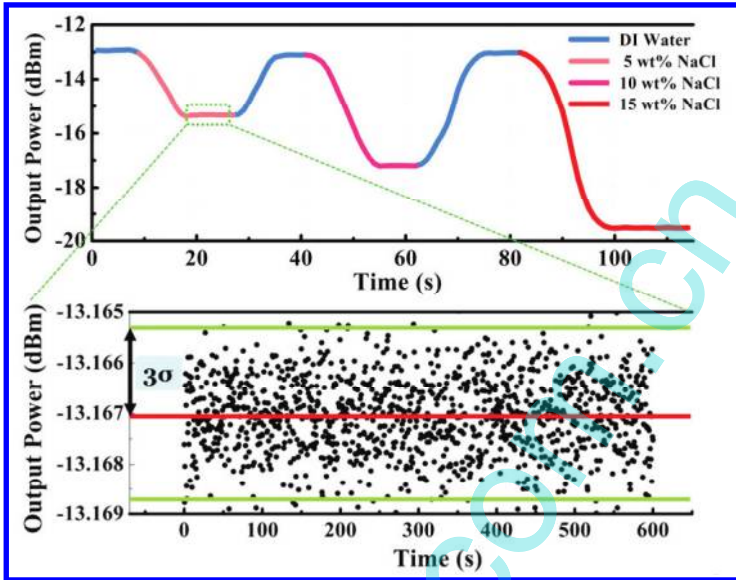

Fig. 12. (Color online) (a) Curve of output power versus time as the alternant injection of DI water and NaCl solutions; (b) determination of standard deviation σ of system noise.

Mod. Phys. Lett. B 2014.28. Downloaded from www.worldscientific.com by UNIVERSITY OF TORONTO on 03/31/14. For personal use only.

www.spm.com.cn

Second, NaCl solutions with concentrations of 5, 10 and 15 wt.% were employed to test the continuous operation of the improved MZI sensor. As is shown in Fig. 12(a), the injections of NaCl solutions in different concentrations with the speed of 2 μL/min cause immediate responses in the transmitted power and the response time for every single measurement is less than 20 s, which means that the hydrophilic property of waveguide surface is effectively improved by the ICP etching in the fabrication of sensing window. We can also observe that once the DI water flushes the microchannels, the output power restores the same value. This repeatability guarantees the accuracy of the refractive measurement and demonstrates the stability of the PDMS flowing chamber and the well control of device fabrication. We know that detecting limit (DL) $= 3\sigma$/sensitivity, where 3σ is the standard deviation of the system.[13] Following the magnification of the measured standard deviation 3σ in Fig. 12(b), the refractive sensing DL in three standard deviations is with the magnitude of 10^{-6} RIU.

5. Conclusion

This paper reported on a comprehensive improvement on the etching conditions for the fabrication of sensing window of MZI waveguide sensor with low-loss and 3D-structure sensing arm, hydrophilic waveguide surface. This optimizing approach along with rapid response and stable operation has rendered the MZI waveguide sensor more competent to practical requirements of RI sensing and biochemical sensing.

Acknowledgments

The authors wish to express their gratitude to the National Natural Science Foundation of China (Nos. 61077041, 61107021, 61177027 and 61261130586), the Ministry of Education of China (Nos. 20110061120052 and 20090061110041), the China Postdoctoral Science Foundation funded project (Nos. 20110491299 and 2012T50297), and the Special Funds of Basic Science and Technology of Jilin University (Nos. 20110315 and 201103076).

References

1. T. Y. Hu, Y. Wang, C. R. Liao and D. N. Wang, *Opt. Lett.* **37** (2012) 5082.
2. B. Y. Li, L. Jiang, S. M. Wang, J. P. Yang, M. M. Wang and Q. H. Chen, *Opt. Laser Technol.* **44** (2012) 640.
3. S. Q. Feng, T. Lei, H. Chen, H. Cai, X. S. Luo and A. W. Poon, *Laser Photon. Rev.* **6** (2012) 145.
4. P. B. Bing, Z. Y. Li, J. Q. Yao, Y. Lu and Z. G. Di, *Mod. Phys. Lett. B* **26** (2012) 1250082.
5. M. S. Luchansky and R. C. Bailey, *Anal. Chem.* **84** (2012) 793.
6. S. V. Pham, M. Dijkstra, A. J. F. Hollink, L. J. Kauppinen, R. M. Ridder, M. Pollnau, P. V. Lambeck and H. J. W. M. Hoekstra, *Sens. Actuators B* **174** (2012) 602.
7. R. G. Heideman and P. V. Lambeck, *Sens. Actuators B* **61** (1999) 100.
8. J. N. Xia, A. M. Rossi and T. E. Murphy, *Opt. Lett.* **37** (2012) 256.
9. S. K. Hong, S. W. Nam and H. J. Yang, *Physica E* **47** (2013) 72.
10. Q. Liu, X. G. Tu, K. W. Kim, J. S. Kee, Y. Shin, K. Han, Y. J. Yoon, G. Q. Lo and M. K. Park, *Sens. Actuators B* **188** (2013) 681.
11. A. L. Washburn and R. C. Bailey, *Analyst* **136** (2011) 227.
12. X. Q. Sun, X. D. Li, C. M. Chen, K. Zhang, J. Meng, X. B. Wang, T. F. Yang, D. M. Zhang, F. Wang and Z. Y. Xie, *Thin Solid Films* **520** (2012) 5946.
13. X. G. Tu, J. F. Song, T. Y. Liow, M. K. Park, J. Q. Yiying, J. S. Kee, M. B. Yu and G. Q. Lo, *Opt. Express* **20** (2012) 2640.

Mod. Phys. Lett. B 2014.28. Downloaded from www.worldscientific.com by UNIVERSITY OF TORONTO on 03/31/14. For personal use only.

www.sdm.com.cn